Polymer 49 (2008) 3785–3794

Contents lists available at ScienceDirect

Polymer

journal homepage: www.elsevier.com/locate/polymer

Hybrid polymer–clay nanocomposites: A mechanical study on gels and multilayered films

Eduard A. Stefanescu [a,*], Cristina Stefanescu [a], William H. Daly [a], Gudrun Schmidt [b], Ioan I. Negulescu [a,c]

[a] Department of Chemistry, Louisiana State University, Baton Rouge, LA 70803, USA
[b] Department of Biomedical Engineering, Purdue University, West Lafayette, IN 47907, USA
[c] School of Human Ecology, Agricultural Center, Louisiana State University, Baton Rouge, LA 70803, USA

ARTICLE INFO

Article history:
Received 14 May 2008
Received in revised form 12 June 2008
Accepted 21 June 2008
Available online 27 June 2008

Keywords:
Composite
Rheology
Film

ABSTRACT

The present contribution describes the preparation and characterization of polymer–clay nanocomposite gels and films containing poly(ethylene oxide) and various ratios of Laponite and Montmorillonite. The aim is to understand how clays with different chemistry, sizes and surface areas interact with each other and affect the structure and characteristics of polymer based nanocomposites in the form of both gels and multilayered films. The rheological behavior of the gels is compared to the spreading process during sample preparation and the resulting film structures and properties are analyzed. While gradually replacing Laponite clay with equivalent amounts of Montmorillonite clay decreases the viscosity of the resulting gels, we observed that the progressive increase of the Montmorillonite percent in the samples leads to a gradual increase of the storage and loss moduli in the multilayered films. At the nano-scale, SAXS and XRD measurements on films indicated that the clay platelets orient parallel to the film plane and that the polymer chains intercalate between silicate galleries. Thermal analysis shows that the polymer crystallinity can be controlled by combination and variation of different clays.

1. Introduction

In recent years a broad literature has emerged that examines the fundamental relationships between network structure, chain dynamics, ionic conductivity and dimensional stability [1] in cross-linked nanosized polymer–clay networks [2–9]. Highly ordered polymer nanocomposites are complex materials that display a rich morphological behavior because of variations in composition, structure, and properties on a nanometer length scale [3,8,9]. Changes in backbone structure, molecular weight, cross-link density, or the introduction of pedant groups can lead to important alterations of polymer segmental motions with a high impact on the thermo-mechanical properties and conductivity of such nanocomposites [9–13]. When the macromolecules are confined to dimensions comparable to their sizes the behavior of polymeric solutions or gels in restricted space can vary greatly from the one in bulk.

Poly(ethylene oxide) (PEO) has been proven to be a valuable candidate for use as an electrolyte host due to its flexible chain structure, beneficial for ionic transport, as well as to its capability to act as a solvent for various metal salts. Due to the retardation of ionic transport imposed by the crystalline phase of PEO, higher ionic conductivity of pure PEO electrolyte can only be achieved in the molten or amorphous state. It has been verified that the addition of nanosized clay fillers with large surface area to PEO dramatically improves its ionic transport characteristics [10,14,15] and its mechanical properties [6,16] on the account of the reduced polymer crystallinity as well as the large interfacial area. Various solutions and melt fabrication techniques leading to materials with intercalated to exfoliated structures have been used for the fabrication of PEO–clay nanocomposites. Since both the polymer (PEO) and the clay (Laponite or Montmorillonite) are hydrophilic in nature no surface treatment is necessary to induce the exfoliation process in solution. Being able to interpenetrate the clay platelets PEO strongly adsorbs to the surface of natural Montmorillonite as well as synthetic Laponite, where the amount of adsorbed polymer is controlled by the layer charge density on the clay [17]. By inducing anisotropy over large length scales in hierarchically structured systems new ways are found for fabricating scientifically novel materials with enhanced thermo-mechanical, optical properties and ionic conductivity [8,9,18,19].

Laponite clay is an inexpensive and environmentally benign disc-shaped silicate with a plate diameter of 25–30 nm and a thickness of approximately 1 nm. In aqueous solutions and gels PEO strongly adsorbs to the charged Laponite nanoparticles

* Corresponding author. Present address: Department of Chemical and Life Science Engineering, Virginia Commonwealth University, Richmond, VA 23284-3028, USA. Tel.: +1 804 827 7000x456; fax: +1 804 828 3846.
E-mail addresses: estefa1@lsu.edu, eastefanescu@vcu.edu (E.A. Stefanescu).

0032-3861/$ – see front matter © 2008 Elsevier Ltd. All rights reserved.
doi:10.1016/j.polymer.2008.06.035

leading to the formation of transparent systems. Smectites such as Montmorillonite are 2:1 charged phyllosilicates that contain exchangeable interlayer cations and show the ability to intercalate various polymers, such as PEO. Montmorillonite clay produces an opaque suspension of predominantly exfoliated platelets that range on average in size from ca. 70 to 100 nm across and are approximately 1 nm thick [8,20–27]. The thickness of Montmorillonite platelets has also been confirmed by AFM measurements [28]. When dispersed alone in water such clays exhibit a Newtonian behavior, but in the presence of polymers the interaction between the polymer chains and the particles causes a major change in the rheological behavior of dispersions [29]. Flow birefringence studies demonstrated that upon shear the clay platelets orient along the flow direction [30,31]. In solution these clay particles can only adsorb a maximum amount of polymer until all the clay surfaces are covered [32]. The polymer and clay build a network-like structure which is interpenetrated by a sub-network of interconnecting pores containing excess polymer and water. During the layer by layer film preparation method the exfoliated solution-structure collapses, reorders and re-intercalates into blob-like chains and layers [8].

The presence of such clays in PEO based polyelectrolytes is advantageous to the improvement of PEO solvating ability towards various Na salts [33]. Having high affinities for water, particularly smectite clays swell to levels that go far beyond their original volumes [4]. Following a similar behavior, polymer–clay nanocomposites exposed to air humidity may exhibit a considerable increase in their size as a result of water adsorption triggered by the pronounced hygroscopic characteristics of these films. The kinetics of water adsorption in polymer–clay polyelectrolytes has been previously studied to correlate the confinement, thickness, crystallinity and melting temperature of the multilayered films with the amount of adsorbed water and water mobility [9,34,35]. More recently, the variation of glass transition temperature of such polymer based nanocomposites has been studied through a theoretical approach, and resulted in a fairly good agreement with experimental data [9,33]. It has been also shown by AFM measurements that the high polydispersity in the size of natural Montmorillonite clay leads to heterogeneities and more defects in orientation of polymer–clay nanocomposites when compared to nanocomposites of similar compositions based on the low disperse, synthetic Laponite clay [8].

The objective of the present contribution is to understand how clays with different chemistry, sizes and surface areas interact with each other and affect the structure and characteristics of polymer based nanocomposites in the form of both gels and multilayered films. The novelty of this study lies in the control of crystallinity by combination and variation of different clays. While earlier studies described alteration of crystallinity by changing the polymer-to-clay ratio [9,10,20,36,37], the polymer molecular weight [9,38], the amount of metal salt [39], and the amount of water [9,40], here we demonstrate that the crystallinity of polymer in such nanocomposites can be tuned by changing the ratio of the two different clays introduced in the systems. In order to search for new synergistic properties and/or improve the properties of nanocomposite solutions and films already known, here we study polymer nanocomposites that have Laponite as well as Montmorillonite incorporated. We combine the gelling and high surface area characteristics of Laponite with the large-aspect-ratio and distinct shear orientation characteristics of Montmorillonite in order to control and suppress crystallinity, and to obtain high levels of orientation that are necessary for enhanced conductivities in such polyelectrolyte films. The rheological behavior of the gels is compared to the spreading process and the resulting film structures and properties are analyzed. At the nano-scale, X-ray scattering experiments (SAXS and XRD) on films are used to investigate structure. The crystallinity in the films is monitored using differential scanning calorimetry (DSC), while the water content in the dry nanocomposites is determined by means of thermogravimetric analysis (TGA). Finally, mechanical properties of the resulted hybrid films are examined through dynamic mechanical analysis (DMA) techniques.

2. Experimental

2.1. Materials and preparation

In this study Laponite-RD (LRD), a synthetic Hectorite type clay, and Montmorillonite clay, Cloisite Na^+ (CNA), (both Southern Clay Products) were used as-received without any further purification. The LRD clay platelets, which are about 25–30 nm across and ca. 1 nm thick charged discs, produce a clear suspension in water. The CNA platelets produce an opaque suspension of predominantly exfoliated platelets that range on average in diameter from 75 to 100 nm across and are ca. 1 nm thick. Poly(ethylene oxide) (PEO) with a molecular mass of 1000 kg/mol ($M_w/M_n = 1.5$) was used as-received from Polysciences Inc. Exfoliated dispersions were prepared by the addition of PEO and Laponite and/or Montmorillonite to deionized water, followed by systematic shaking, mixing and centrifuging for at least four weeks. The solution pH and ionic strength were controlled by the addition of NaOH (pH ≈ 9) and NaCl (5.5×10^{-2} M), respectively. At rest and room temperature most dispersions are gels (except for LRD0–CNA3–PEO2, which is a viscoelastic fluid). Each multilayered film was prepared by manually spreading the hydrogel on a glass slide with a spatula. In the past we have shown that reproducible results are obtained when using and comparing two preparation techniques: (i) a simple spreading device can be used that guarantees the same thickness of each spread layer and (ii) the films are spread manually with a blade [8]. Every 1.5–2 h one layer was spread and dried under ambient conditions. Overnight, samples were dried in desiccators. On average, five layers were spread every day. While one spread and dried film (7 μm ± 2 μm) already produces multilayers we used sequential absorption to obtain thicker films simply for better investigation and handling [2,24,25,41]. Films with the same spreading direction were dried layer by layer one on top of another until a total thickness of about 0.25 mm was obtained for the multilayered film. After the last layer was spread and half dried the thin multilayered film was placed in a vacuum oven and dried overnight at 25 °C. The sample was then removed from the oven and placed in a desiccator for storage and further drying. Following this procedure a set of five LRD–CNA–PEO gels were prepared with compositions described in Table 1. All gels contain 95% water, 2% PEO and 3% clay, where the only difference from a sample to

Table 1
Nanocomposite gels and films: composition (by weight) and crystallinity

	Sample name[a]	LRD (wt%)	CNA (wt%)	PEO (wt%)	Crystallinity (%)
LRDX%–CNA(3 − X)%–PEO2% – gels (gels contain 95% water)					
1	LRD0–CNA3–PEO2	0	3	2	N/A
2	LRD0.75–CNA2.25–PEO2	0.75	2.25	2	N/A
3	LRD1.5–CNA1.5–PEO2	1.5	1.5	2	N/A
4	LRD2.25–CNA0.75–PEO2	2.25	0.75	2	N/A
5	LRD3–CNA0–PEO2	3	0	2	N/A
LRDX%–CNA(60 − X)%–PEO40% – films (after water evaporation)					
1	LRD0–CNA60–PEO40	0	60	40	30
2	LRD15–CNA45–PEO40	15	45	40	21
3	LRD30–CNA30–PEO40	30	30	40	10
4	LRD45–CNA15–PEO40	45	15	40	1
5	LRD60–CNA0–PEO40	60	0	40	0

[a] The samples were abbreviated LRD*X*–CNA*y*–PEO*z*, where *x*, *y*, and *z* denote the weigh fraction of Laponite, Montmorillonite and poly(ethylene oxide), respectively, either in solution or in the multilayered film.

another consists in the ratio of Laponite/Montmorillonite used to prepare each gel. By evaporating the water in the drying process the final films result with compositions of 40% polymer and 60% clay, being also characterized by different Laponite/Montmorillonite ratios as illustrated in Table 1. The same sample preparation procedure has been used for all five samples.

2.2. Rheological experiments

Oscillatory and steady state shear rheology measurements of nanocomposite gels were performed on a stress controlled TA Instruments AR1000 Rheometer. A cone-and-plate geometry with a diameter of 40 mm, a gap of 27 μm, and a cone angle of 0°59′54″ was used for all determinations. The instrument was equipped with a solvent trap to prevent water evaporation. All rheological measurements were conducted at a temperature of 25 °C and within one week after the preparation of gels to avoid the appearance of any time dependent transitions in the gels. Duplicate measurements for both viscosity and moduli (G', G'') measurements show good reproducibility with a relative uncertainty of ≈7%.

2.3. X-ray scattering (SAXS) measurements

Small angle scattering data were obtained at the Center for Advanced Microstructures and Devices (CAMD, Baton Rouge, Louisiana) at the SAXS beamline ($6a_1$). The beamline is equipped with an LNLS (Laboratorio Nacional de Luz Synchrotron, Brazil) double crystal monochromator with a practical energy range of 2–16 KeV, and is computer interfaced and controlled. The scattering data were collected with $\lambda = 2.10$ Å. In a standard *Z*-beam configuration the incident beam is perpendicular to the spread direction and parallel to the plane of the film, and SAXS intensity is obtained in the *X*–*Y* plane (see Fig. 5 for definition of planes). In the *Y*-beam configuration the incident beam is perpendicular to the plane of the multilayered film and intensity is obtained in the *X*–*Z* plane.

2.4. X-ray diffraction (XRD) measurements

The X-ray diffraction measurements were done using a Siemens–Bruker D5000 X-ray diffractometer with a Cu Kα radiation of 1.54 Å. Diffraction patterns were collected from $2\theta = 2°$ to $2\theta = 50°$ with steps of 0.02° and a scan time of 2 s per step. All collected data were normalized to the same baseline for a better comparison of final results. Samples were dried and kept in desiccators before each measurement.

2.5. Differential scanning calorimetry (DSC) and thermogravimetric analysis (TGA) measurements

DSC measurements were performed on a TA 2920 MDSC instrument. Samples of 8–10 mg were subjected to analysis using a heating rate of 10 °C/min in two successive heating cycles. For all DSC curves negative going features correspond to endothermic processes. For each measurement, a fresh nanocomposite sample was used in the first heating run followed by cooling and then a second heating run. TGA measurements were performed in nitrogen atmosphere with a heating rate of 10 °C/min using a TA 2950 thermo-balance. Only fresh samples of 7–10 mg were subjected to thermogravimetric analysis. TA Universal analysis software was used for the integration and processing of all curves resulted from DSC and TGA instruments.

2.6. Dynamic mechanical analysis (DMA)

The glass transition temperature (T_g) and complex, storage and loss moduli (E^*, E', E'') of the thin nanocomposite films were determined via DMA measurements using a Rheometrics Scientific ARES instrument equipped with a torsion rectangular tool, a heating oven and a liquid nitrogen controller. Samples of 0.25 mm thickness and 6–7 mm width were subjected to various oscillatory tests. Results were normalized to the same transversal section, 1 mm^2, to allow comparison. All DMA measurements were conducted at 25 °C except for the glass transition temperature measurements. Duplicate measurements show very good reproducibility with a relative uncertainty of ≈5%.

3. Results and discussion

3.1. Characterization of nanocomposite gels: rheological measurements

The rheological behavior of nanocomposite gels was studied to identify the relationship existing between gels' composition and their performance under shear, as well as to observe the variation of storage and loss moduli as a function of clay type in the nanocomposite dispersions. Viscosity experiments are presented in Fig. 1a in an attempt to correlate the shear orientation in the gels with the final orientation in the dried films. As observed in previous work for similar gels [26,31], shear thinning behavior is observed over a wide range of shear rates. It can be noticed that at the same clay/PEO ratio Laponite clay leads to the formation of gels more viscous than the ones containing only Montmorillonite clay.

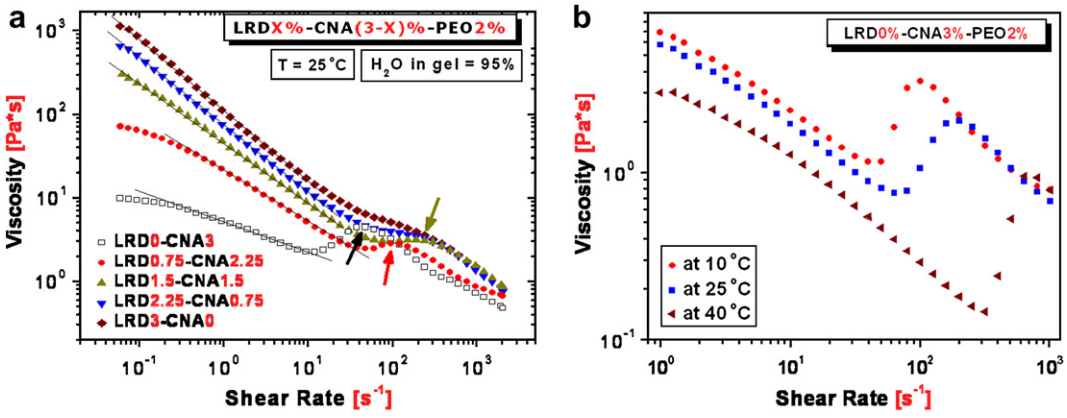

Fig. 1. (a) Viscosity values as a function of shear rate for LRD*X*–CNA(3 − *X*)–PEO2 nanocomposite gels (95% water) at 25 °C; (b) viscosity values as a function of shear rate for LRD0–CNA3–PEO2 at different temperatures. Relative uncertainty is ≈7%.

Gradually replacing Laponite with equivalent amounts of Montmorillonite decreases the viscosity of the gel. This decrease in viscosity is more evident at low shear rates. A remarkable feature in Fig. 1a is the occurrence of a transition in the system at shear rates higher than 10^1 s^{-1}. The transition shifts to higher shear rates as more Laponite is added to the gel, replacing Montmorillonite. For LRD0–CNA3–PEO2, LRD0.75–CNA2.25–PEO2 and LRD1.5–CNA1.5–PEO2 samples the transition (indicated by arrows) results in a sudden increase in viscosity, the magnitude of which decreases with the increase of the Laponite percent. For gels containing Laponite amounts higher than 1.5% (Laponite-to-Montmorillonite ratio > 1) the transition does not lead to an increase in viscosity but rather to a decrease in the magnitude of the shear thinning behavior. The transition is also temperature dependent, as indicated for LRD0–CNA3–PEO2 in Fig. 1b, where an increase in temperature shifts the transition peak to higher shear rates. In addition to shifting the transition shear rates, temperature has also an effect on the magnitude of the transition, where higher temperatures result in larger transitions.

At lower shear rates, before reaching the transition domain, there is a near linear relationship between the $\log(\eta)$ and $\log(d\gamma/dt)$, as evidenced by the solid lines in Fig. 1a. This indicates that over the shear rate dependent region the solutions are power law fluids that exhibit shear thinning behavior. The power law relation can be expressed as $\eta = m(d\gamma/dt)^{n-1}$, where η is the shear viscosity (Pa s), m is the consistency index, $d\gamma/dt (d\gamma/dt = \dot{\gamma})$ is the shear rate (s^{-1}), and n is the power law index and has values comprised between 0 and 1. Higher degrees of shear thinning result in n values closer to 0, while n values closer to 1 indicate a solution behavior approaching the one of Newtonian fluids [29]. Power law indexes are in the range of: $n = 0.2(\pm 0.03)$ for LRD3–CNA0–PEO2 and LRD2.25–CNA0.75–PEO2, $n = 0.3(\pm 0.03)$ for LRD1.5–CNA1.5–PEO2, $n = 0.4(\pm 0.03)$ for LRD0.75–CNA2.25–PEO2 and $n = 0.5(\pm 0.03)$ for LRD0–CNA3–PEO2. Clearly the shear thinning behavior is enhanced as the concentration of Laponite in the clay mixtures increases.

Frequency dependent oscillatory shear experiments of LRDX–CNA$(3 - X)$–PEO2 samples are presented in Fig. 2. The data were collected at strains within a relatively broad viscoelastic range. Although all gels contain 95% water the storage modulus G' always appears larger than the loss modulus G'' (except for LRD0–CNA3–PEO2 at low frequencies) indicating elastic behavior. All samples show some frequency dependence of the modulus G', which increases with increasing frequency. Both moduli G' and G'' are observed to increase when increasing the percent of Laponite in the sample. No crossover frequency could be observed for any of the Laponite-containing samples. For LRD0–CNA3–PEO2 sample the crossover of G' with G'' occurs at a frequency of 2 Hz.

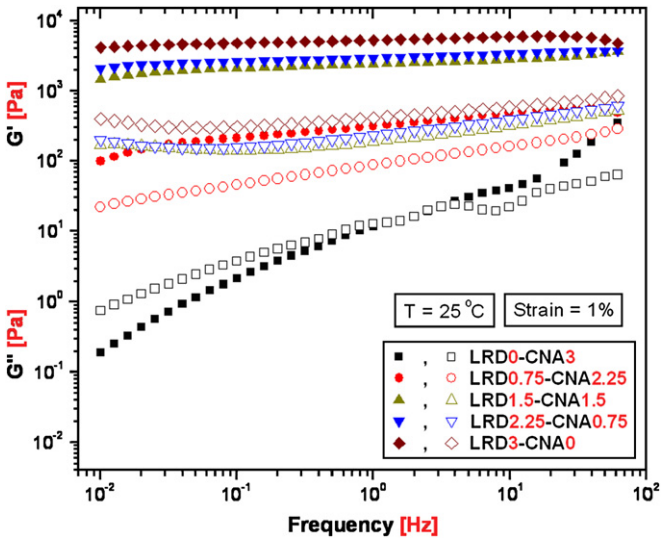

Fig. 2. Frequency dependence of G' and G'' for LRDX–CNA$(3 - X)$–PEO2 gels of various Laponite–Montmorillonite compositions; G' data are represented with filled symbols and G'' data are shown with empty symbols. All gels contain 2% PEO and 95% water. Relative uncertainty is ≈7%.

From previous studies we know that polymers that are long enough to form inter-particle bridges promote the formation of a reversible polymer–clay network that dominates the rheological response [26,31,42]. At rest, all polymer–clay samples consist of a network between randomly oriented clay platelets and PEO chains with polymer chains acting as dynamic cross-links between the platelets (see Fig. 4 when system is at rest). As shown by Mongondry et al., in the presence of PEO the steric hindrance of chains adsorbed onto the clay particles inhibits aggregation of particles [43]. Although several parameters such as surface chemistry, dimensional polydispersity, degree of exfoliation, impurities or affinity of PEO to the clay may affect the rheology of gels, in these systems the major contribution to the viscosity behavior exhibited by the gels appears to be the relative distributions of the surface areas for the two types of clay. Due to their small diameter, for a given mass, the more numerous completely exfoliated Laponite platelets provide a larger effective surface available for coordination with the surrounding PEO chains than a corresponding weight of Montmorillonite clay. With diameters three to four times larger, fewer exfoliated Montmorillonite platelets exist in the same mass. However, since the platelet thickness for the two types of clay is virtually the same (1 nm), the increase in the relative surface area for the smaller Laponite platelets consists mainly of edge surfaces, but not top surfaces. So the surface area alone cannot be the factor responsible for the behavior of viscosity. The major factor responsible for the increase in the viscosity of Laponite rich gels is the improved distribution of surface area (available for PEO coordination) in the system. The total surface of one Montmorillonite platelet corresponds to the surface area of roughly four Laponite platelets. Statistically, the number of configurations and/or orientations that the four Laponite platelets (viewed as a whole) can adopt in the gel with respect to the PEO chains is significantly larger than the number of configurations of a single Montmorillonite platelet. This fact is exemplified in Fig. 3 where four PEO chains are shown to interact with either two Montmorillonite platelets (a) or with eight Laponite platelets (b). The improved distribution of the Laponite surface area leads to the formation of many favorable "polymer–clay" configurations that will lead to polymer–clay coordination (cross-links). If the number of Laponite and/or Montmorillonite platelets and PEO chains in Fig. 3 was further increased (e.g. 4 CNA platelets/8 PEO chains and 16 LRD platelets/8 PEO chains), the number of cross-links in each dispersion would increase proportionally and the difference between the two systems would become even more obvious. This improved cross-linking in PEO–Laponite systems leads to the formation of stronger polymer–clay networks, with many coordinated PEO chains, and little excess uncoordinated PEO [26,31]. The stronger network is the reason why Laponite rich gels exhibit viscosities and shear moduli higher than Montmorillonite rich gels (Figs. 1a and 2). The long polymer dangling ends observed when PEO interacts with Montmorillonite platelets (Fig. 3a) will later be shown to crystallize during the film drying process.

Shear thinning of our gels typically indicates the occurrence of an overall orientation of the macrostructures and/or nanostructures in the gel. Under shear the clay platelets orient along the flow direction with the surface normal to vorticity direction [44]. The overall orientational alignment in the system is a competition between flow alignment and configurational relaxation, where the flow alignment is induced by orientation of platelets and stretching

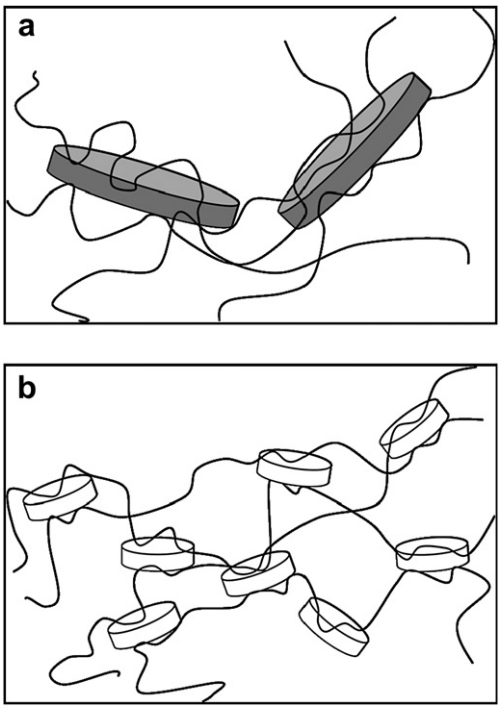

Fig. 3. Schematic showing the interactions of four PEO chains with two Montmorillonite platelets (a), and eight Laponite platelets (b). Despite the fact that the area provided by the faces of the eight Laponite platelets is equivalent to the area provided by the faces of the two Montmorillonite platelets, the Laponite platelets lead to the formation of more polymer–clay cross-links due to a better spatial distribution of the total surface. The better interaction of polymer chains with Laponite platelets leads to the formation of stronger networks characterized by high viscosities and storage moduli.

of polymer chains under shear. The schematic in Fig. 4 shows the behavior of polymer–clay dispersions that we think to occur during the rheological experiment. When the dispersion is initially loaded in the rheometer (before applying shear to the sample) the entire system is at rest, and the sample consists of a network between randomly oriented clay platelets and PEO chains with polymer chains acting as dynamic cross-links between the platelets. At the shear rate just below the critical shear rate the PEO chains are fully stretched and the platelets are aligned in the shearing direction. With a further increase of the shear rate the critical shear rate is reached, and the adsorption/desorption equilibrium is broken. At this point the desorption of chains from the platelets surface occurs at a higher rate than adsorption does. The desorbed polymer chains, now floating free in the system, will recoil (Fig. 4) in order to reach

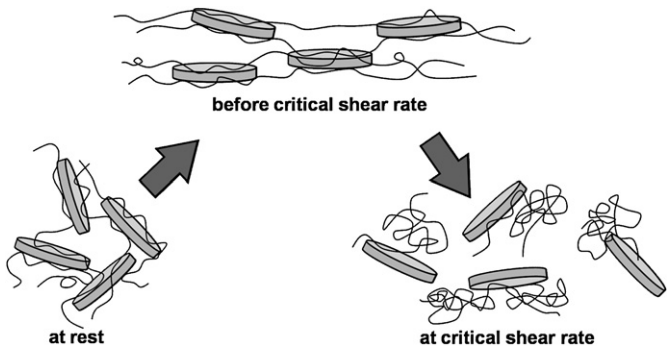

Fig. 4. Schematic showing the behavior of nanostructures in polymer–clay dispersions at three different stages during the rheological experiment.

a more favorable thermodynamic state, impairing the flow in the gel. In the same time the orientation of nano-platelets is disturbed, also perturbing the flow of the system. In this way, the configurational relaxation gradually increases with the shear rate and negatively affects the overall orientational alignment in the system, leading to the appearance of a transition. Since Montmorillonite rich networks are much weaker than Laponite rich networks the configurational relaxation for the former systems occurs at lower shear rates, and to a greater extent, making the larger transition-peak shift to the left (Fig. 1a).

The change in the rheological properties with temperature is due to several factors, among which the most important is that relaxation times decrease strongly as the temperature increases [45,46]. Due to these smaller relaxation times the onset and the peak shear rates of the unsteady shear flow transitions are shifted to higher values as the temperature increases. In addition to this, the increase of the overall entropy in the gel with temperature, which translates into an amplified disorder in the system, triggers the increase in the magnitude of the transition at higher temperatures (Fig. 1b).

3.2. Characterization of nanocomposite films prepared from gels

3.2.1. SAXS and XRD measurements

Due to the ordering imposed in the shear spreading process the clay platelets are expected to be oriented with the surface parallel to the plane of the film, as indicated in the schematic shown in Fig. 5. In order to study the orientation of clay platelets in the film, SAXS measurements were carried out for two orientations of the sample with respect to the X-ray beam. The SAXS results from the five multilayered films are presented in Fig. 6. The isotropic SAXS pattern in the *X*–*Z* plane and the anisotropy observed in the *X*–*Y* plane (see Fig. 5 for definition of planes) for all films confirm the orientation of the platelets to be with the surface parallel to the plane of the film. From the two-dimensional (2D) SAXS patterns (i–v) presented in Fig. 6 the intensity as a function of q in the *Z* and *Y* directions was calculated and plotted. The plot in Fig. 6a shows the intensity obtained from the edge (beam coming from the *Z*-direction) of the five nanocomposite films. A remarkable feature in this plot is the appearance of a peak (indicated by arrows) in all curves at $q \approx 0.4\ \text{Å}^{-1}$. The peak corresponds to a *d*-spacing ($d_{SAXS} = 2\pi/q$) in the order of 15.7 Å and it is related to the distance between stacked clay platelets containing intercalated PEO. The differences in the *d*-spacing given by the SAXS measurements (15.7 Å) and XRD measurements (17.5 Å) presented in Fig. 7a, are attributed to the differences in the wavelength of the X-rays used by the two instruments (2.10 Å in SAXS vs. 1.54 Å in XRD). The complete absence of this intercalation peak (at $q \approx 0.4\ \text{Å}^{-1}$) from the *Y*-direction SAXS curves presented in Fig. 6b reinforces the hypothesis that the clay platelets are oriented with the surface parallel to the plane of the film (as shown in Fig. 5).

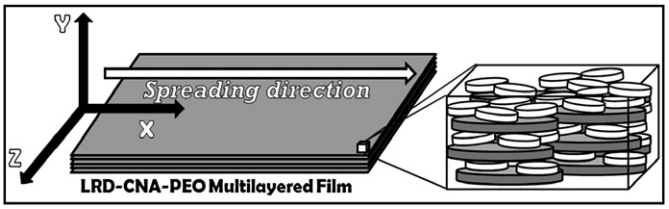

Fig. 5. General idealized clay platelet orientation in a multilayered polymer–clay film presented along with the definition of planes. The large discs represent the Montmorillonite platelets, while the small ones indicate the Laponite platelets. Note that the diameter of Montmorillonite platelets is 3–4 times larger than the one of the Laponite particles. The PEO chains have been omitted for clarity.

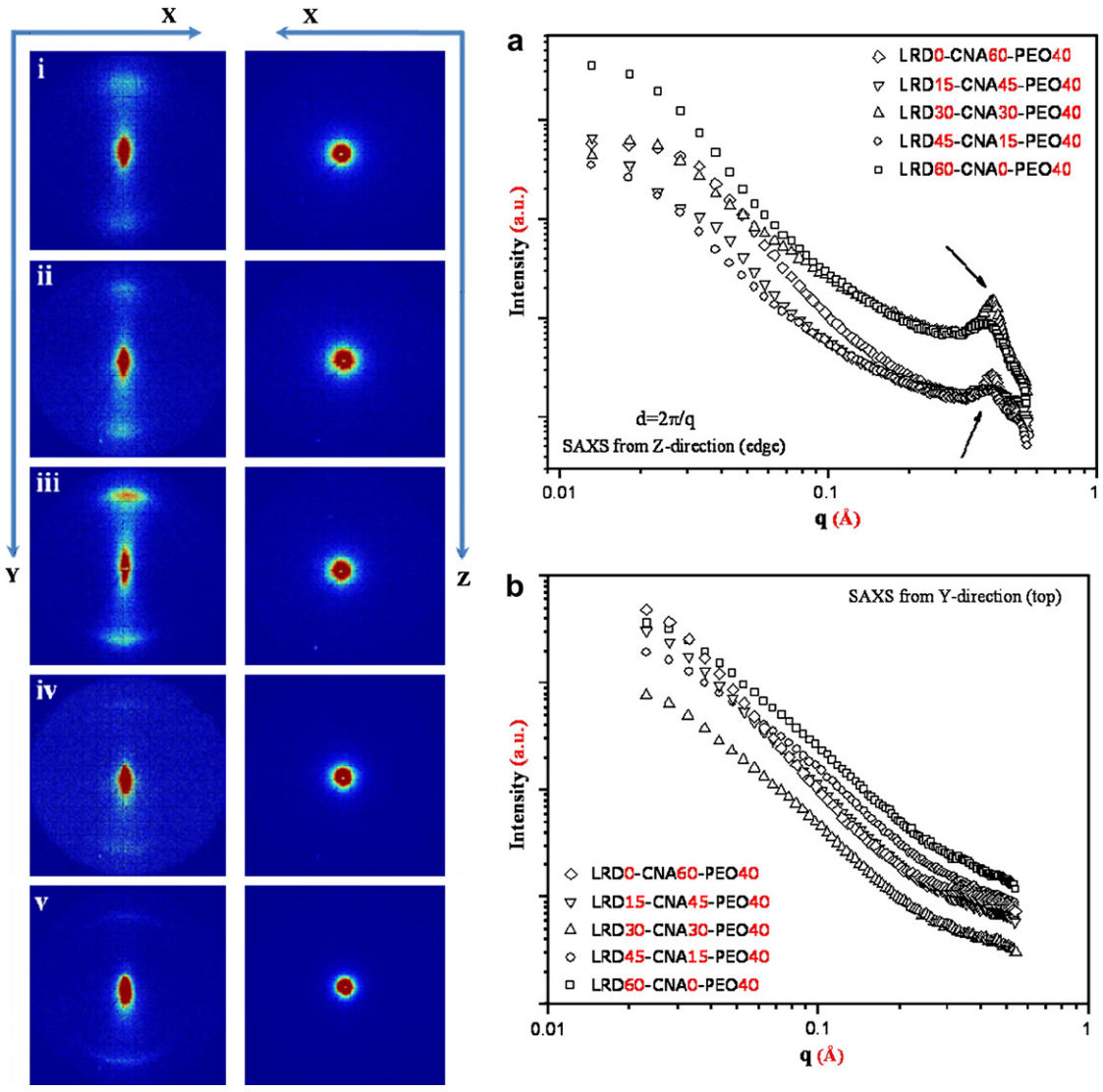

Fig. 6. SAXS patterns from the *Z* and *Y* directions for LRD60–CNA0–PEO40 (i), LRD45–CNA15–PEO40 (ii), LRD30–CNA30–PEO40 (iii), LRD15–CNA45–PEO40 (iv) and LRD0–CNA60–PEO40 (v). The intensity as a function of *q* is also presented for SAXS measurements from the *Z*-direction (a), and from the *Y*-direction (b).

X-ray diffraction patterns of LRD*X*–CNA(60 − *X*)–PEO40 films are presented in Fig. 7a. Although the polymer–clay solutions from which the nanocomposite films are made are predominantly exfoliated [8], XRD confirms that all our dried multilayered films are highly structured. The X-ray reflections predominantly correspond to the PEO intercalated clay suggesting the presence of polymer–clay stacks in the system. Intercalation of PEO chains between the clay platelets can be deduced by comparing the *d*-spacing values from the XRD reflections of the layered pure Laponite and layered pure Montmorillonite clays with the *d*-spacing values from the XRD reflections of the layered nanocomposites (Fig. 7b). The intercalation peak for all the nanocomposites corresponds to a *d*-spacing of about 17.5 Å, a result in agreement with what has been previously found in literature for similar systems [9,47,48]. The *d*-spacing values of the pure Laponite and pure Montmorillonite are around 11.5 Å (Fig. 7b). The LRD containing films show a slightly higher (0.5 Å) *d*-spacing of platelets than CNA films. The difference in the *d*-spacing between polymer nanocomposites and pure clays (≈6 Å) is attributed to the presence of PEO chains between the clay platelets.

The thickness of a nanocomposite crystal involved in the diffraction process can be conveniently determined from the width of the peak at half-height (a careful distinction has to be made between a PEO crystallite or crystal, constructed from ordered PEO chains only, and a nanocomposite crystal, made of intercalated PEO–clay stacks) [49]. A quantitative measure of the nanocomposite crystal involved in the diffraction process is given by the Scherrer equation, which can be used to estimate crystal size if the crystal is smaller than 100 nm [50–52].

$$L = \lambda K/\beta\cos\theta$$

In this equation L is the mean crystal dimension (expressed in Å) along a line perpendicular to the reflecting plane, K is a constant close to unity ($K = 0.94$), and β is the width of a peak at half-height expressed in radians of 2θ (width measured in 2θ degrees and then multiplied by $\pi/180$). The calculated values of the crystal thickness (L) as resulted from the Scherrer equation for the intercalation peaks observed in Fig. 7a are as follows: for *LRD0–CNA60–PEO40* $L = 172$ Å, for *LRD15–CNA45–PEO40* $L = 127$ Å, for *LRD30–CNA30–PEO40* $L = 101$ Å, for *LRD45–CNA15–PEO40* $L = 84$ Å, and for *LRD60–CNA0–PEO40* sample $L = 59$ Å. The data indicate that increasing the amount of Laponite in the system results in a decrease of thickness of the crystal involved in the diffraction process. Such a behavior is

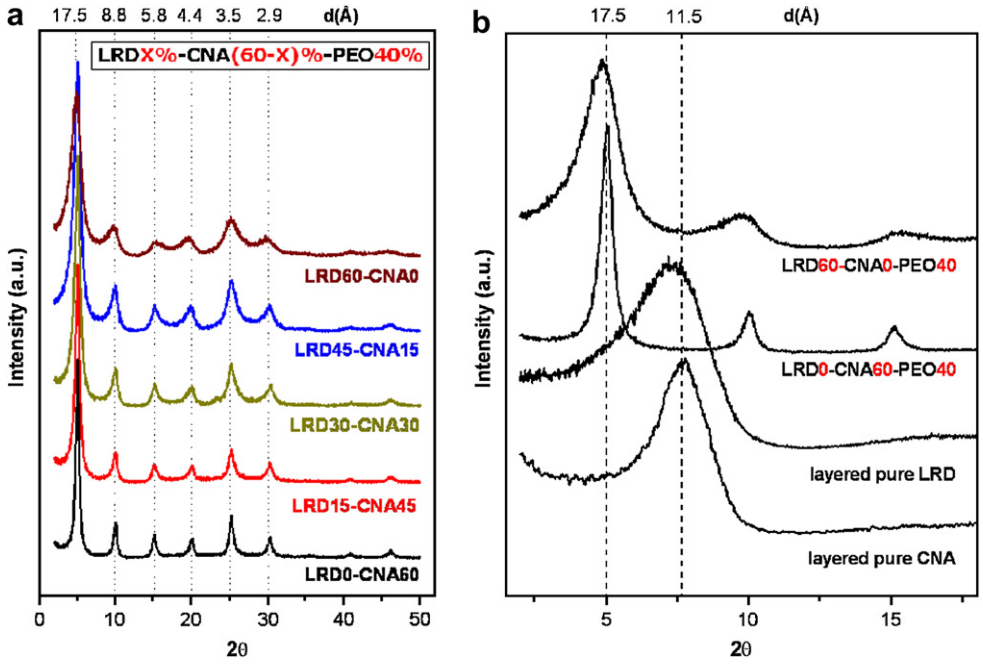

Fig. 7. (a) XRD patterns of LRD*X*–CNA(60 – *X*)–PEO40 nanocomposite films of different Laponite–Montmorillonite compositions; (b) XRD patterns for LRD60%–PEO40% and CNA60%–PEO40% nanocomposites and for the layered pure Laponite (LRD) and Montmorillonite (CNA) clays.

expected, since the low-aspect-ratio Laponite platelets have difficulties in maintaining order and parallelism inside a polymer–clay crystal (when compared to the high-aspect-ratio Montmorillonite platelets) [49].

3.2.2. DSC and TGA measurements

To better understand the intimate relationship between composition of nanocomposite films and their mechanical properties, we have observed the polymer crystallinity in the systems by means of DSC (Fig. 8a and Table 1). Although extensive studies have been previously done on the crystallinity of various bulk PEO nanocomposites at low clay concentration [17,20,53], here we focus on anisotropic materials at high clay concentrations. DSC thermograms were obtained in the second heating cycle of the DSC measurement to avoid artifacts that could influence the results. This procedure removes mechanical tensions that may originate from the layering process during film formation. Measurements that were done on LRD*X*–CNA(60 – *X*)–PEO40 nanocomposites (Fig. 8a and Table 1) indicate that gradually replacing Montmorillonite clay with equivalent amounts of Laponite results in a gradual decrease of crystallinity up to a point where all the polymers become completely amorphous in the sample (LRD60–CNA0–PEO40 sample). If we consider the crystallinity of our bulk PEO ($\Delta H = 118.9$ J/g, resulted from DSC) relative to the endotherm observed in the films, then PEO in the LRD0–CNA60–PEO40 sample is only 30% as crystalline as the bulk polymer. Crystallinity numbers decrease in increments proportional to the percent clay replaced in the system (Table 1). We expect the clay confined polymer to be amorphous since the coordination of PEO oxygens to various cations from the surface of the platelets disrupts the chain order and limits their possibility to move and rearrange [27,36]. Our results suggest that the high surface/gram ratio, triggered by the small size of Laponite platelets, as well as the uniform distribution of surface area with respect to the polymer, provides the PEO chains with a confinement area large enough to totally suppress their crystallinity

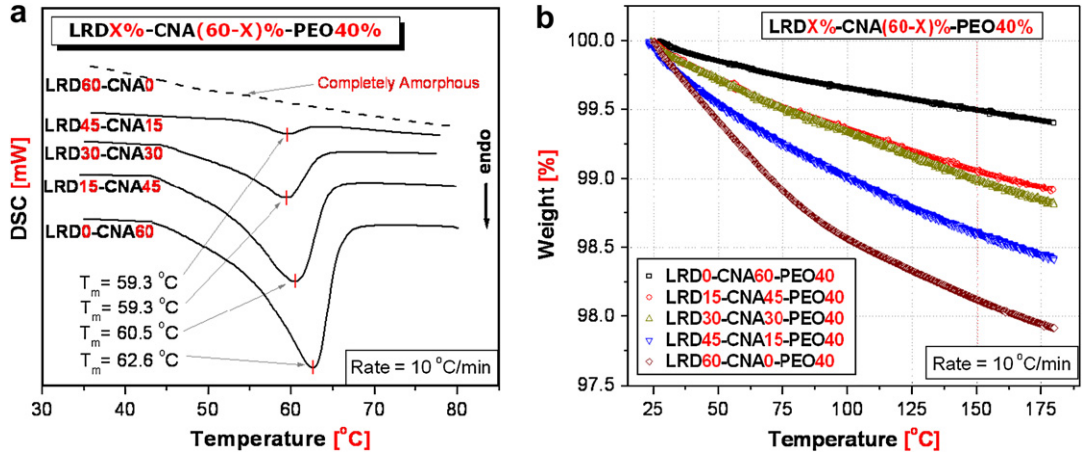

Fig. 8. DSC (a) and TGA (b) traces for LRD*X*–CNA(60 – *X*)–PEO40 nanocomposite thin films at a heating rate of 10 °C/min. All films contain 40% PEO.

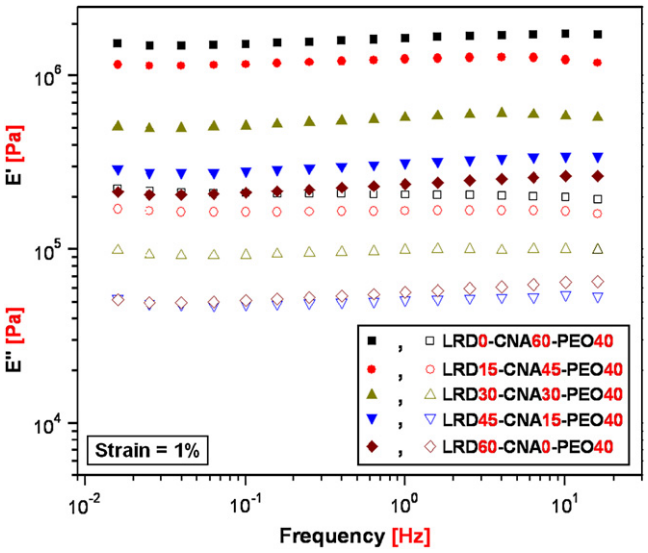

Fig. 9. Frequency dependence of storage modulus (E') and loss modulus (E'') for LRDX–CNA($60-X$)–PEO40 nanocomposite thin films. E' data are represented with filled symbols and E'' data are shown with empty symbols. Relative uncertainty is ≈5%.

(LRD60–CNA0–PEO40 sample). In contrast, the larger Montmorillonite platelets from the LRD0–CNA60–PEO40 sample only suppress the PEO crystallinity by 70% relative to the pure polymer.

When polymer chains are adsorbed to the clay layers, water molecules initially present on the silicate surfaces and galleries are displaced to accommodate the polymer chains. Although the nanocomposite films have been dried in vacuum, some water molecules may still be trapped in the films, as indicated by TGA measurements (Fig. 8b). Displaced water molecules from the clay surfaces, or water molecules from the precursor solutions, are likely trapped within PEO crystallites, shifting the melting transition to lower temperatures (Fig. 8a) [54]. The trend observed in the TGA plot also indicates that Laponite rich films retain higher amounts of water than Montmorillonite rich films. The high affinity of PEO chains towards water makes complete removal of these small molecules from the dried films very difficult, even when films are stored in desiccators for several weeks. One can see that a higher PEO crystallinity results in a lower polymer affinity for water molecules (Fig. 8b) due to the close packing of the macromolecular chains.

3.2.3. DMA measurements

Although complex (E^*), elastic (E') and loss (E'') moduli of solid films are dependent on many parameters, in this work we only study their behavior as a function of testing frequency, temperature and time. The storage (E') and loss (E'') moduli of the five nanocomposite films are presented in Fig. 9 as a function of testing frequency. All storage and loss moduli have somewhat reduced values (in the range of 10^6 Pa) due to the small transversal area (1 mm^2) that was used to normalize the results. It can be observed that the progressive increase of the Montmorillonite percent in the sample leads to a gradual increase of E' and E'' values in the multilayered films. The complex modulus (E^*) values of the multilayered films are presented in Fig. 10a and b as a function of frequency, at two different oscillation amplitudes (strain %). Comparing Fig. 10a and b, one can clearly see that an increase in the oscillating amplitude, from 0.1 to 1%, results in a considerable decrease of E^* for all the samples. Similar to the behavior observed for E' at 1% strain (Fig. 9), the E^* of the nanocomposites at this oscillating amplitude (Fig. 10b) increases with increasing the Montmorillonite fraction in the sample. However, at oscillating amplitudes of 0.1%, despite having a lower Montmorillonite percent, the LRD15–CNA45–PEO40 sample shows a complex modulus higher than the one of LRD0–CNA60–PEO40 samples, for the entire frequency range studied here. Furthermore, at 10 Hz, the E^* of the completely amorphous LRD60–CNA0–PEO40 sample equals the one of the LRD45–CNA15–PEO40 samples, and it is expected to exceed this value at even higher frequencies (Fig. 10a). Due to the instrument limitations, measurements at frequencies higher than 15 Hz could not be conducted.

The behavior of E' and E'' observed for the multilayered films in Fig. 9 is totally opposite to the one observed for the storage (G') and loss (G'') moduli of the precursor nanocomposite gels (Fig. 1a). While the factor responsible for the elevation of G' and G'' in gels was the increase in the strength of the polymer–clay network, here the main reason for the elevation of E' and E'' in the films consists in the increase in crystalline fraction of the PEO in the nanocomposite (other factors that may influence E' of films, such as temperature, pressure, film thickness and width, polymer polydispersity, polymer molecular weight, and platelet orientation, are maintained the same for all five films). Since the strength of the network in solution is given by the fraction of PEO chains cross-linked to the clay platelets, which cannot rearrange and crystallize, it follows that the strength of the network is inversely proportional to the fraction of crystalline PEO in the film. The increase in the crystallinity of the samples is also responsible for the increase of E^* (Fig. 10a and b),

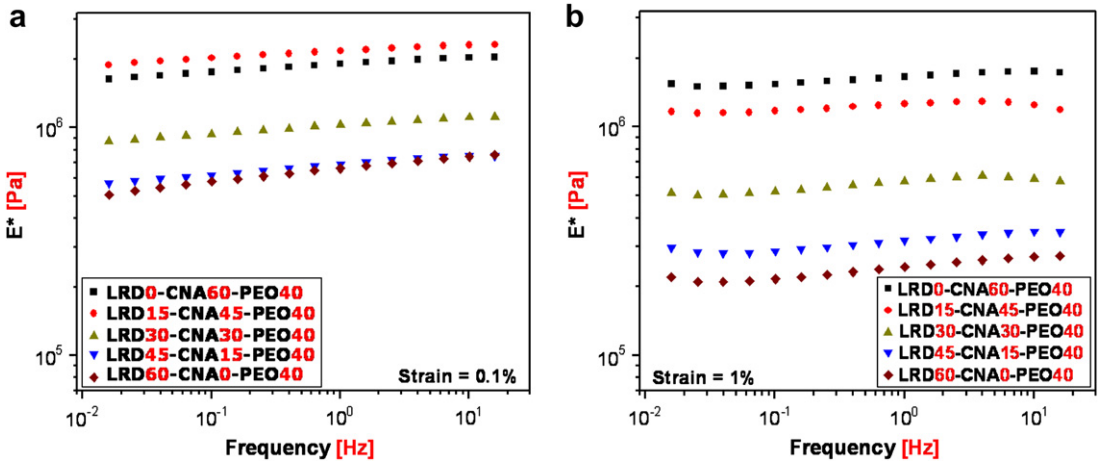

Fig. 10. Dependence of complex modulus (E^*) for LRDX–CNA($60-X$)–PEO40 nanocomposite thin films on (a) frequency at 0.1% strain; (b) frequency at 1% strain. Relative uncertainty ≈5%.

given that at 25 °C E^* is essentially E'. Another factor responsible for the reduction of E' and E'' (when increasing the Laponite content) could be the presence of higher amounts of water in Laponite rich films (indicated by the TGA plot in Fig. 7). However, we believe that the contribution of water is limited, since the amounts of moisture incorporated in the films are less than 2% (wt/wt) as indicated by TGA at 150 °C (Fig. 7). In addition to crystallinity and moisture variations an important contribution to the overall behavior of E' and E^* of the films could also be brought by the general orientation of nano-platelets in the composite multilayered films. One would expect highly oriented films to exhibit an increased toughness, and in consequence, an enhanced E'. The large-aspect-ratio of the Montmorillonite clay may play a decisive role in maintaining the polymer covered platelets parallel and aligned in the same direction throughout several length scales [49]. The much smaller Laponite platelets might have difficulties in maintaining parallelism throughout several length scales in the film, and high amounts of this clay in the nanocomposite may lead to a decrease in the storage modulus, E'.

For the frequency dependence of E^* at 1% strain (Fig. 10b) excellent reproducibility was achieved when measurements were each time repeated on a fresh sample. However, while attempting to do a second determination on samples already tested at this oscillating amplitude we observed that the thin films break and the results cannot be reproduced. To elucidate the behavior of nanocomposite films under prolonged stress a set of time dependent measurements of E^* were conducted, the results of which are presented in Fig. 11. At the oscillating amplitude of 1% the nanocomposites experience severe deformations, which set off the appearance of small micro-cracks on the surface of the films. In time and under oscillating stress these micro-cracks grow bigger, link with each other and form macro-cracks, which lead to an important loss of material strength, triggering the decrease in E^*. Further deformations irreversibly lead to the fracture of the nanocomposite films (points indicated by arrows in Fig. 11). One can notice that the nanocomposites containing only one type of clay, as in the case for LRD0–CNA60–PEO40 and LRD60–CNA0–PEO40, have a better resistance to fatigue than the rest of tested materials. We attribute this improved fatigue resistance of samples containing only one type of clay to an increased homogeneity of the systems, generated by a consistent size and surface area of the nano-platelets.

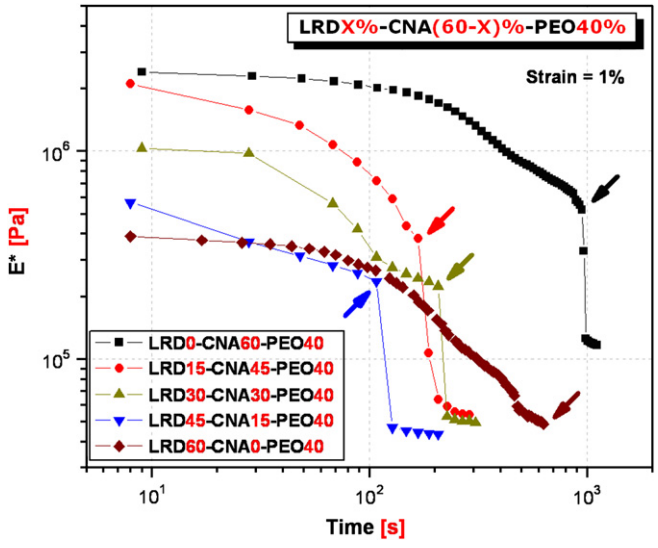

Fig. 11. Dependence of complex modulus (E^*) for LRDX–CNA(60 − X)–PEO40 nanocomposite thin films on time at 1% strain and a frequency of 10 rad/s. Arrows indicate the failure points for the five nanocomposites. All films contain 40% PEO. Relative uncertainty is ≈10%.

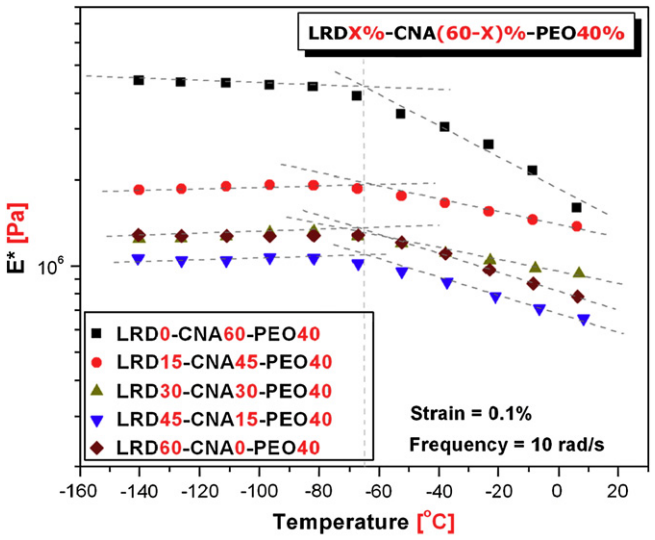

Fig. 12. Dependence of complex modulus (E^*) for LRDX–CNA(60 − X)–PEO40 nanocomposite thin films on temperature. All films contain 40% PEO. Relative uncertainty is ≈5%.

The temperature dependence of complex modulus of nanocomposite thin films is presented in Fig. 12 for a frequency of 10 rad/s and a strain of 0.1%. A horizontal plateau followed by a gradual decrease of E^* with the temperature can be observed for all the samples. The glass transition temperature, at which the decrease of E^* begins, was found to be −66 °C, value that has been previously reported in literature for PEO [55]. Due to the small PEO percent in the nanocomposites (40%), and to the very small thickness of the films (0.25 mm), the loss modulus (E'') curves, and in consequence the tan δ curves, for all the studied samples resulted very noisy for the entire temperature range, even when measurements were repeated. For the temperature range presented in Fig. 12 E^* is virtually the same with E' due to the high rigidity of the samples at these temperatures. The small deformations used here (0.1% strain) allowed the measurements to be repeated on the same sample up to four times, without damaging the nanocomposite films. Surprisingly, E^* of the completely amorphous LRD60–CNA0–PEO40 sample shows values higher than the one of the LRD45–CNA15–PEO40 samples, which contains a small fraction of crystalline polymer (Table 1). In the past we have shown that the high polydispersity of natural Montmorillonite (CNA) clay leads to heterogeneities and more defects in orientation compared to the low disperse synthetic Laponite (LRD) clay [8]. The more compact structure of the Montmorillonite-free LRD60–CNA0–PEO40 film is able to compensate for the lack of polymer crystallinity and to exhibit a complex modulus higher than the one of LRD45–CNA15–PEO40 samples at this range of temperatures.

4. Conclusion

We have shown that the mechanical behavior of polymer–clay nanocomposite dispersions and multilayered films can be tuned by controlling the ratio of Laponite-to-Montmorillonite in the materials. The shear thinning behavior is enhanced and the viscosity increases as the relative concentration of Laponite increases in gels. A progressive increase of the relative Montmorillonite percent in the samples leads to a gradual increase in the storage and loss moduli, E' and E'', of the multilayered films. We oppine that the factor responsible for the elevation of G' and G'' in gels is the

increase in the strength of the polymer–clay network. On the other hand, the elevation of E' and E'' in multilayered films is due to the increase in crystalline fraction of the PEO in the nanocomposites, since other parameters that might influence E' and E'' (such as temperature, pressure, film thickness and width, polymer polydispersity, polymer molecular weight, and platelet orientation) were maintained the same for all multilayered films.

Acknowledgements

This research was partially funded by LSU Agricultural Center. We thank Southern Clay Products for providing the Montmorillonite and Laponite clays that were used in this work. Cristina Stefanescu thanks Derek Dorman of LSU for help with the SAXS measurements.

References

[1] Pinnavaia TJ, Beall GW. Polymer–clay nanocomposites. Chichester, UK: John Wiley & Sons Ltd; 2000.
[2] Dundigalla A, Lin Gibson S, Ferreiro V, Malwitz MM, Schmidt G. Macromol Rapid Commun 2005;26:143.
[3] Elmahdy MM, Chrissopoulou K, Afratis A, Floudas G, Anastasiadis SH. Macromolecules 2006;39:5170.
[4] Inyang HI, Bae S, Mbamalu G, Park S-W. J Mater Civ Eng 2007;19(1):84.
[5] Loiseau A, Tassin JF. Macromolecules 2006;39:9185.
[6] Loyens W, Maurer HJF, Jannasch P. Polymer 2005;46:7334.
[7] Qiu WL, Pyda M, Nowak-Pyda E, Habenschuss A, Wunderlich B. Macromolecules 2005;38:8454.
[8] Stefanescu EA, Dundigalla A, Ferreiro V, Loizou E, Porcar L, Negulescu I, et al. Phys Chem Chem Phys 2006;8:1739.
[9] Stefanescu EA, Schexnailder PJ, Dundigalla A, Negulescu II, Schmidt G. Polymer 2006;47:7339.
[10] Chen H-W, Chiu C-Y, Wu H-D, Shen I-W, Chang F-C. Polymer 2002;43:5011.
[11] Gournis D, Floudas G. Chem Mater 2004;16:1686.
[12] Khatua BB, Lee DJ, Kim HY, Kim JK. Macromolecules 2004;37:2454.
[13] Lin J-J, Chen Y-M. Langmuir 2004;20:4261.
[14] Croce F, Appetecchi GB, Persi L, Scrosati B. Nature 1998;394:456.
[15] Doeff MM, Reed JS. Solid State Ionics 1998;113–115:109.
[16] Loyens W, Jannasch P, Maurer FHJ. Polymer 2004;46:915.
[17] Bujdak J, Hackett E, Giannelis EP. Chem Mater 2000;12:2168.
[18] Gadjourova Z, Andreev YG, Tunstall DP, Bruce PG. Nature 2001;412:520.
[19] Gadjourova Z, Marero DM, Andersen KH, Andreev YG, Bruce PG. Chem Mater 2001;13:1282.
[20] Chaiko DJ. Chem Mater 2003;15:1105.
[21] Ho DL, Briber RM, Glinka CJ. Chem Mater 2001;13:1923.
[22] Lee KM, Han CD. Polymer 2003;44:4573–88.
[23] Maiti M, Bhowmick AK. Polymer 2006;47:6156.
[24] Malwitz MM, Dundigalla A, Ferreiro V, Butler PD, Henk MC, Schmidt G. Phys Chem Chem Phys 2004;6:2977.
[25] Malwitz MM, Lin-Gibson S, Hobbie EK, Butler PD, Schmidt G. J Polym Sci Part B Polym Phys 2003;41:3237.
[26] Stefanescu EA, Petrovan S, Daly WH, Negulescu II. Macromol Mater Eng 2008; 293(4):303–9.
[27] Strawhecker KE, Manias E. Chem Mater 2003;15:844.
[28] Ploehn HJ, Liu C. Ind Eng Chem Res 2006;45:7025.
[29] Arias CB, Zaman AA, Talton J. J Dispersion Sci Technol 2007;28:247.
[30] Schmidt G, Nakatani AI, Butler PD, Karim A, Han CC. Macromolecules 2000;33: 7219.
[31] Schmidt G, Nakatani AI, Han CC. Rheol Acta 2002;41:45.
[32] Loizou E, Butler PD, Porcar L, Talmon Y, Kesselman E, Schmidt G. Macromolecules 2005;38:2047.
[33] Zhang H, Zhao Y, Wang J, Zheng H. J Phys Chem C 2007;111:5382.
[34] Vogt BD, Soles CL, Jones RL, Wang C-Y, Lin EK, Wu W-l, et al. Langmuir 2004; 20:5285.
[35] Vogt BD, Soles CL, Lee HJ, Lin EK, Wu WL. Langmuir 2004;20:1453.
[36] Chen H-W, Chang F-C. Polymer 2001;42:9763.
[37] Rao YQ, Blanton TN. Macromolecules 2008;41:935.
[38] Edman L, Ferry A, Doeff MM. J Mater Res 2000;15:1950.
[39] Elmer AM, Jannasch P. Polymer 2005;46:7896.
[40] Aranda P, Mosqueda Y, Perez-Cappe E, Ruiz-Hitzky E. J Polym Sci Part B Polym Phys 2003;41:3249.
[41] Malwitz MM, Butler PD, Porcar L, Angelette DP, Schmidt G. J Polym Sci Part B Polym Phys 2004;42:3102.
[42] Loizou E, Butler P, Porcar L, Schmidt G. Macromolecules 2006;39:1614.
[43] Mongondry P, Nicolai T, Tassin J-F. J Colloid Interface Sci 2004;275:191–6.
[44] Schmidt G, Nakatani AI, Butler PD, Han CC. Macromolecules 2002;35:4725.
[45] Morrison FA. Understanding rheology. New York, 10016: Oxford University Press, Inc.; 2001.
[46] Nielsen LE. In: Mechanical properties of polymers and composites, vol. 1. Marcel Dekker, Inc; 1974.
[47] Vaia RA, Vasudevan S, Krawiec W, Scanlon LG, Giannelis EP. Adv Mater 1995; 7:154.
[48] Zhao Q, Samulski ET. Macromolecules 2003;36:6967.
[49] Stefanescu EA, Daly WH, Negulescu II. Macromol Mater Eng 2008; doi:10.1002/mame.200800081.
[50] Cullity BD. Elements of X-ray diffraction. USA: Addison-Wesley Publishing Company, Inc.; 1978.
[51] Moore DM, Reynolds RCJ. X-ray diffraction and the identification and analysis of clay minerals. 198 Madison Avenue, New York, NY 10016: Oxford University Press, Inc.; 1997.
[52] Warren BE. X-ray diffraction. NY 11501, USA: Dover Publications, Inc.; 1990.
[53] Ratna D, Divekar S, Samui AB, Chakraborty BC, Banthia AK. Polymer 2006;47: 4068.
[54] Aranda P, Ruiz-Hitzky E. Appl Clay Sci 1999;15:119.
[55] Cowie JMG. Polymers: chemistry and physics of modern materials. Cheltenham, UK: Nelson Thornes Ltd; 1991.